Article

Structure

Glycan Activation of a Sheddase: Electrostatic Recognition between Heparin and proMMP-7

Graphical Abstract

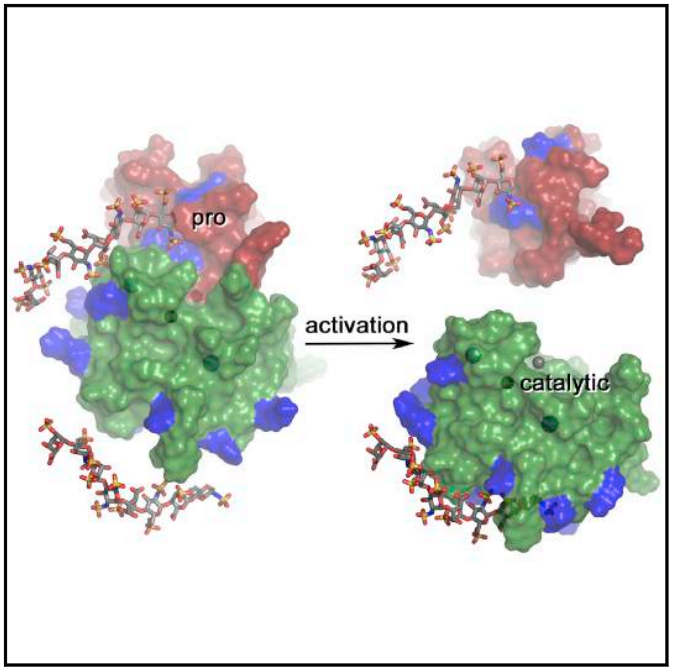

Authors

Yan G. Fulcher, Stephen H. Prior, Sayaka Masuko, ..., Fuming Zhang, Robert J. Linhardt, Steven R. Van Doren

Correspondence

vandorens@missouri.edu

In Brief

Glycosaminoglycans recruit the protease MMP-7 to growth factors, receptors, and antibacterial proteins for maturation and shedding from cell surfaces. Fulcher et al. orient heparin chains on basic strips on the zymogen using NMR in solution and mutations that interfere in heparin-triggered maturation.

Highlights

- Heparin oligosaccharides bind two basic tracks and pockets of proMMP-7
- Both modes of binding support proteolytic maturation of the zymogen
- Heparin chains perturb the termini of proMMP-7
- Allostery and shedding may be attributed to GAG binding remote on catalytic domain

Accession Numbers

5UE2
5UE5

Fulcher et al., 2017, Structure *25*, 1100–1110
July 5, 2017
http://dx.doi.org/10.1016/j.str.2017.05.019

CellPress

Structure
Article

Glycan Activation of a Sheddase: Electrostatic Recognition between Heparin and proMMP-7

Yan G. Fulcher,[1] Stephen H. Prior,[1,3] Sayaka Masuko,[2] Lingyun Li,[2] Dennis Pu,[2] Fuming Zhang,[2] Robert J. Linhardt,[2] and Steven R. Van Doren[1,4,*]

[1]Department of Biochemistry, University of Missouri, 117 Schweitzer Hall, Columbia, MO 65211, USA

[2]Department of Chemistry and Chemical Biology, Center for Biotechnology and Interdisciplinary Studies, Rensselaer Polytechnic Institute, Troy, NY 12180, USA

[3]Present address: School of Chemistry, College of Science, University of Lincoln, Brayford Pool, Lincoln, Lincolnshire LN6 7TS, UK

[4]Lead Contact

*Correspondence: vandorens@missouri.edu

http://dx.doi.org/10.1016/j.str.2017.05.019

SUMMARY

Heparan sulfate proteoglycans activate the matrix metalloproteinase-7 zymogen (proMMP-7) and recruit it in order to shed proteins from cell surfaces. This occurs in uterine and mammary epithelia, bacterial killing, lung healing, and tumor cell signaling. Basic tracks on proMMP-7 recognize polyanionic heparin, according to nuclear magnetic resonance and mutations disruptive of maturation. Contacts and proximity measurements guided docking of a heparin octasaccharide to proMMP-7. The reducing end fits into a basic pocket in the pro-domain while the chain continues toward the catalytic domain. Another oligosaccharide traverses a basic swath remote on the catalytic domain and inserts its reducing end into a slot formed with the basic C terminus. This latter association appears to support allosteric acceleration of proteolysis. The modes of binding account for extended, heterogeneous assemblies of proMMP-7 with heparinoids during maturation and for bridging to pro-α-defensins and proteoglycans. These associations support proteolytic release of activities at epithelial cell surfaces.

INTRODUCTION

Heparan sulfate (HS) is a key type of polyanionic glycosaminoglycan (GAG) that binds at least 300 human extracellular and cell surface proteins (Ori et al., 2011; Xu and Esko, 2014). These species are often active in development and inflammation. Some cysteine proteases, aspartic proteases, serine proteases, and metalloproteinases are activated by GAGs, with accompanying proteolytic removal of the pro-domain (Theocharis et al., 2014). The regulatory effects on cancers of interactions of GAGs with basic patches on proteases led to the proposal of targeting these interactions as a potential therapeutic strategy (Theocharis et al., 2014). Among the matrix metalloproteinases (MMPs), GAGs activate MMP-2 (Crabbe et al., 1993) and MMP-7 (Ra et al., 2009). GAG chains or proteoglycans harboring them bind to the hemopexin-like domain of MMP-2 (Iida et al., 2007), MMP-9 (Malla et al., 2013), and MMP-13 (Zhang et al., 2010). However, MMP-7 (matrilysin) lacks such a domain. Both the pro- and catalytic domains of proMMP-7 bind heparinoid chains (Fulcher et al., 2014). However, the locations and orientations of binding have been unclear.

MMP-7 was recognized to bind heparan sulfate proteoglycans (HSPGs) on epithelial cell surfaces (Yu and Woessner, 2000). GAG-MMP-7 interactions in mucosa activate bacterial killing in the intestine (Ra et al., 2009; Wilson et al., 1999), wound healing in the lung (Chen et al., 2009; Gill et al., 2016; Gill and Parks, 2008; Li et al., 2002; Parks et al., 2001), and signaling and remodeling in uterine and mammary epithelia (Yu et al., 2002) and epithelial tumors (Fingleton et al., 1999; Lynch et al., 2007; Mitsiades et al., 2001; Vargo-Gogola et al., 2002). GAG chains draw MMP-7 together with pro-α-defensin for proteolytic activation to its bactericidal form (Ra et al., 2009). The GAG chains of CD44 at cell surfaces co-localize MMP-7 with pro-HB-EGF for activation to HB-EGF, which then binds its ErbB4 receptor on uterine, mammary, and tumor epithelia (Yu et al., 2002). The HSPG known as syndecan-2 binds proMMP-7 on human colon adenocarcinoma cells and activates it to mature MMP-7, which can shed syndecan-2 from the surface of these cells (Ryu et al., 2009). MMP-7 governs neutrophil localization, activation, and resolution of neutrophilic inflammation by shedding complexes of syndecan-1 with murine CXCL1 (KC, or the human ortholog CXCL8) (Chen et al., 2009; Gill et al., 2016; Hayashida et al., 2009; Li et al., 2002). Analogous to these cellular processes, GAG chains that are 16 residues or longer link proMMP-7 molecules together such that they activate neighboring zymogens in *trans* within aggregate assemblies (Fulcher et al., 2014). Octasaccharides instead promote formation of simpler, monodisperse complexes. Deletion of the C-terminal KRSNSRKK sequence also inhibits heparinoid-promoted assembly and activation of proMMP-7 (Fulcher et al., 2014).

HS from cell surfaces and its degradation product of heparin (Choi et al., 2012; Hartmann-Petersen et al., 2009; Li et al., 2002; Yu et al., 2002) exhibit an extended, anionic polymeric structure of repeating disaccharides of 1–4-linked uronic acid and α1–4-linked D-glucosamine (Conrad, 1998; Khan et al., 2010; Xu and Esko, 2014). HS is highly variable in length and sulfation, whereas heparin is more enriched in sulfation and typically 12–14 kDa (Xu and Esko, 2014). HS has greater

N-acetylation. Heparin is produced commercially as a biopharmaceutical and serves as the experimental surrogate for HS (Xu and Esko, 2014). Heparin oligosaccharides of defined length are useful for structural studies of protein-GAG interactions (Capila and Linhardt, 2002; Muñoz and Linhardt, 2004; Xu and Esko, 2014).

Two paramagnetic nuclear magnetic resonance (NMR) approaches that accurately define protein-protein interfaces were adopted herein for defining protein-glycan interfaces. One method affixes a nitroxide spin label to one partner and measures its close approaches to the other partner as NMR line broadenings known as paramagnetic relaxation enhancements (PREs) (Clore, 2015). The other approach uses a freely diffusible Gd(III) chelate to introduce solvent PREs to the protein surface. The exposure and solvent PREs at the surface are compared with and without the partner bound (Arumugam et al., 1998; Madl et al., 2011). This is accurate for associations of modest affinity (Garimella et al., 2006), which is pertinent to some protein-carbohydrate interactions.

Using paramagnetic NMR in this study improved investigation of the hypothesis of Yu and Woessner (2000) that a cradle of positive charge around the back of the catalytic domain of rat MMP-7 binds heparin or HS. Both the pro-domain and the basic C-terminal octapeptide from the catalytic domain of human MMP-7 are critical for the binding of heparinoids and maturation of the zymogen to the active form (Fulcher et al., 2014). Heparinoid binding and allosteric enhancement of catalytic velocity remain after removal of the C-terminal peptide and pro-domain, implying another binding site in the catalytic domain that supports the positive allosteric modulation (Fulcher et al., 2014). This allosteric effector site can be hypothesized to lie within the basic arc. We tested the ability of positively charged residues in these regions to recruit heparinoid chains productively to human proMMP-7 using NMR, site-directed mutagenesis, and assays of heparin-induced maturation of proMMP-7. Docking calculations using the measured contacts define an arc of allosteric GAG binding to the back of the catalytic domain of human MMP-7 and a binding site bridging between domains. GAG binding to the former site most probably (1) links mature MMP-7 to multiple proteins it matures or sheds from epithelial cell surfaces and (2) induces the allosteric enhancement of catalytic velocity. Both binding trajectories promote GAG-triggered maturation of proMMP-7.

RESULTS

Heparin 8-mers Perturb Remote and Catalytically Important Residues

Heparin-binding sites and affinity for proMMP-7 were sought using NMR in solution. ^{15}N-labeled proMMP-7, inactivated by E195A replacement of the general base, was titrated with a homogeneous heparin octasaccharide (dp8) (Figure S1). ^{15}N-transverse relaxation optimized spectroscopy (TROSY) NMR spectra were collected with additions of heparin dp8 (Figure S2A) with 140 mM NaCl present. The heparin dp8-induced shifts of the amide NMR peaks (chemical shift perturbations [CSPs]) in the pro-domain map to surface patches at Gly5 and Gly6 and Tyr25, Lys30, and Asn31, as well as the autoinhibitory loop (Figures 1A and 1B). Perturbed residues buried in the autoinhibitory loop are Met62, Cys67 (zinc ligand), and Asp71 (salt-bridged to Arg66). On the opposite side of the catalytic zinc, heparin dp8 shifts the amide NMR peak of catalytic residue 195. The responses of residues 67, 71, and 195 around the active site suggest propagation of allosteric effects from the binding site.

Heparin dp8 induces small CSPs at Ser76 and Leu77, perhaps suggesting conformational adjustment in the exposed linker that is digested during maturation (Figures 1A and 1B). Heparin dp8 induces larger shifts of the amide peaks of Phe149 and Lys247 at the interface with the pro-domain, as well as at Leu108, Met115, Lys118, and Ser227 that cluster on the back of the catalytic domain (Figures 1A and 1B). The largest heparin dp8-induced CSPs map to an adjacent surface patch comprising Val89, His123, Arg125, and Lys126 (Figures 1A and 1B). The basic residues in these latter two patches and a patch on the pro-domain suggest potential sites of contact with heparin oligosaccharides, a prospect investigated further below.

The CSPs are progressive and initially proportional to the heparin dp8 added (Figure 1C), indicating chemical exchange that is fast on the NMR chemical shift scale. However, protein precipitation and severe line broadening began at 1.5-fold molar excess of heparin dp8, before full saturation. Fitting of a simple binding isotherm (Equation 1 in STAR Methods) to the shifts of the amide peak of Cys67 suggests an apparent dissociation constant (K_D) of 63 ± 9 μM (Figure 1C). Global fitting of a binding isotherm instead to the shifts of the NMR peaks of five residues in the catalytic domain suggests slightly weaker apparent K_D of 83 ± 4 μM. The binding isotherm derived by principal component analysis of lists of all peaks of the zymogen (Sakurai and Goto, 2007; Xu and Van Doren, 2016, 2017) is best fitted by a K_D of 70 ± 5 μM (Figure 1D).

Without NaCl present, heparin dp8 induces shifts of amide NMR peaks that are larger than those in near-physiological saline solution (Figure S3A). These CSPs are prominent for Lys30, Cys67, Val89, His123, Arg125, Lys126, Ala195, and Lys247, suggesting the similarity of the binding sites with and without NaCl. The additional CSPs of Thr104, Ile120, and Leu122 without NaCl (Figure S3A) might suggest a wider swath of heparin dp8 binding to the back of the catalytic domain. Without NaCl, about 0.5 molar equivalents of heparin dp8 appear to saturate the association. This agrees with the observations of two zymogens binding per heparin dp8 chain under low-salt conditions (Fulcher et al., 2014). Fits to the binding isotherms of the titration suggest apparent K_D to be in the range of 2–5 μM when correcting an overly simplistic 1:1 binding model (Equation 1) for the precipitation that occurs without NaCl. The sensitivity of the affinity to [NaCl] corroborates the electrostatic nature of the recognition.

Basic Side Chains That Assist the C Terminus in Heparin Association

We hypothesized that candidate sites for interactions with polyanionic heparin are positively charged side chains near backbone amide groups with NMR peaks shifted by heparin dp8. To test this idea, we prepared site-directed mutations of 14 such basic residues marked in Figure 2A. For GAG-triggered activation assays, the point mutations were prepared in active wild-type (wt) and ΔC backgrounds, where ΔC refers to the

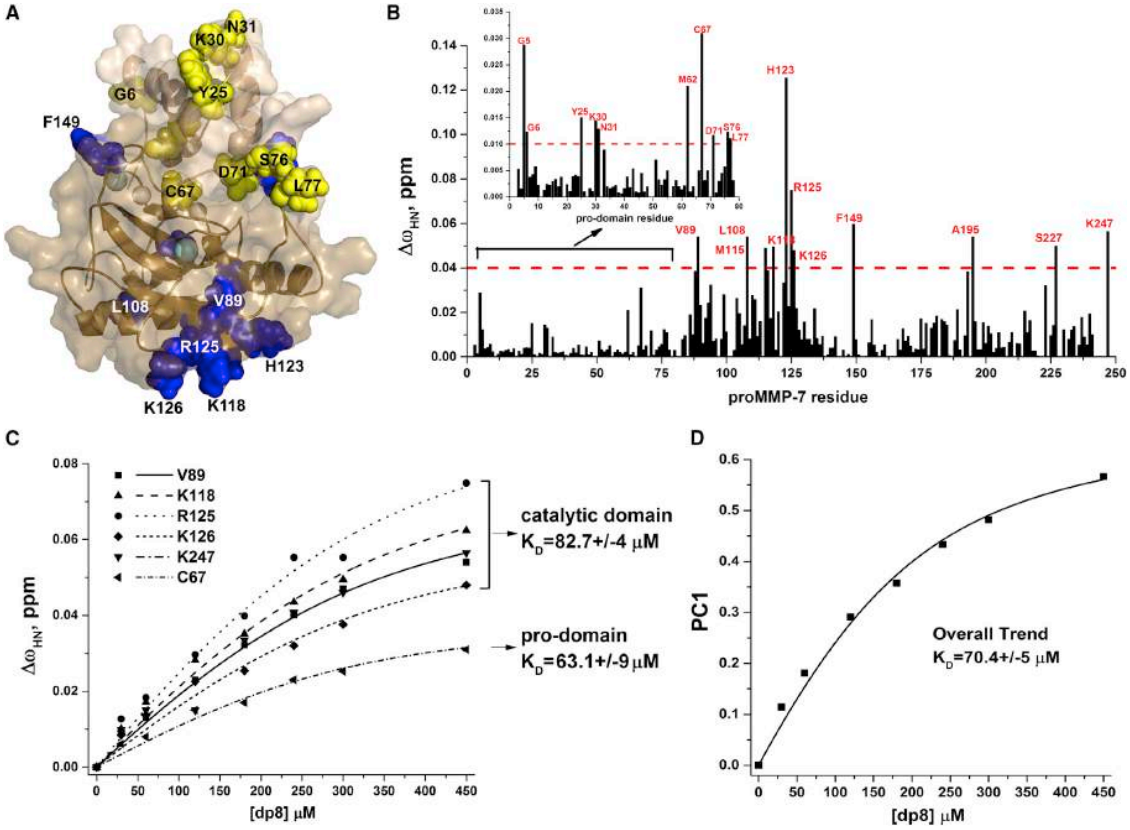

Figure 1. NMR Peaks of proMMP-7 Shifted by Heparin dp8 Suggest Binding Sites and Affinity

(A) Residues with amide peaks shifted most by heparin dp8 in nearly physiological saline are colored yellow on the pro-domain and blue on the catalytic domain of the NMR structure of proMMP-7(E195A) (Prior et al., 2015). The thresholds for selecting residues to plot are amide chemical shift changes (Equation 1) with $\Delta\omega_{HN}$ > 0.01 ppm in the pro-domain and >0.04 ppm in the catalytic domain, which are 2 SDs above the mean for the respective domain. See Figure S1 for the structure and isolation of heparin dp8.

(B) The chemical shift perturbations of ^{15}N-BEST-TROSY spectra of proMMP-7(E195A) by 1.5-fold molar excess of heparin dp8 are plotted versus residue number. The inset expands the changes in the pro-domain. See Figure S2 for TROSY spectra at the beginning and end of a titration with the octasaccharide.

(C) Heparin dp8-induced amide chemical shift changes of six residues of the catalytic domain (fitted globally) and one in in the pro-domain are plotted as a function of [dp8]. See Figure S3 for a titration in the absence of NaCl.

(D) An overall binding isotherm was obtained from principal component (PC) analysis of peak picks of the spectra (Xu and Van Doren, 2016).

deletion of the C-terminal KRSNSRKK sequence. For assays of binding to a heparin-coated surface using surface plasmon resonance (SPR), ten of the mutations were prepared in backgrounds inactivated by E195A or E195A/ΔC. K20A and K30A substitutions, without or with ΔC, do not significantly affect binding (Figure 2B). The alanine substitutions around the large helix of the catalytic domain at Arg92, Arg107, Lys111, Arg125, Lys126, or close to the pro-domain at Arg177 decreased the extent of binding to the heparin-coated surface (Figure 2B). The R107A, R111A, and R125A + K126A substitutions compromised binding the most, suggesting that they could be central to the main binding site. Combining ΔC with the R125A + K126A lesion only modestly enhanced impairment of binding; this non-additivity suggests proximity in these residues' interactions with heparin, based on guidelines for the interpretation of double mutations (Wells, 1990). The ΔC deletion amplified disruption of heparin binding by substitutions of other basic residues in the catalytic domain. Combination of ΔC with R92A, R107A, or K111A is most disabling to heparin association (Figure 2B). Sizable decreases in binding to the heparin chip by combining ΔC with alanine replacements of Lys87, Arg92, Arg98, Arg107, Lys118, Arg140, or Arg177 suggest additivity and independence of these positions from the C terminus in heparin interactions.

Basic Side Chains Fostering Heparin-Induced *trans*-Activation of proMMP-7

We sought to determine which sites of heparin interactions are functionally important. We evaluated which of the basic residues provide the electrostatic attraction that is productive for activation of the zymogen. We tested the effects of site-directed

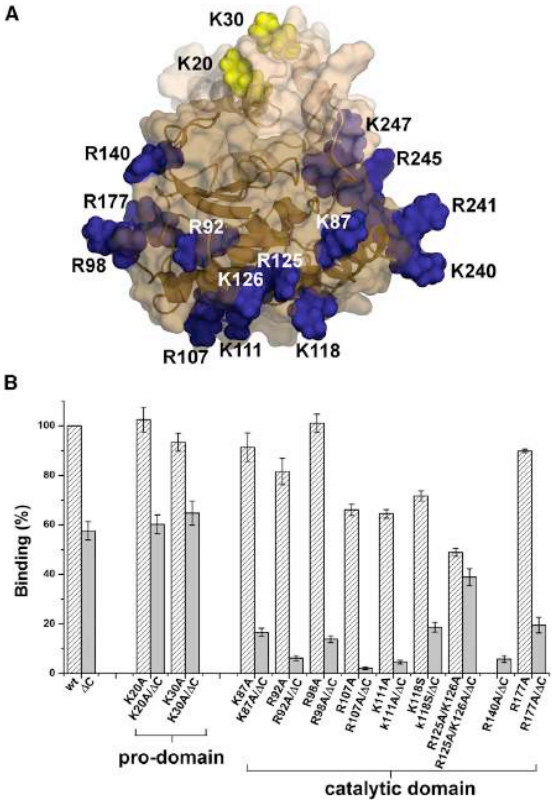

Figure 2. Impact on Heparin Affinity of Alanine Substitutions for Positive Charges

(A) The basic residues targeted by mutagenesis are colored yellow on the pro-domain and blue on the catalytic domain on the NMR structure.

(B) The amounts of binding to a heparin-coated chip are compared among wild-type (wt) proMMP-7(E195A), single mutations (striped columns), and the point mutations combined with the deletion of C-terminal basic peptide deletion denoted ΔC (gray columns). The amplitude of the response units of each association was normalized (Zhang et al., 2009) to the scale of full binding (100%) by the positive wt control of proMMP-7(E195A). The mean and SD of triplicate measurements are reported.

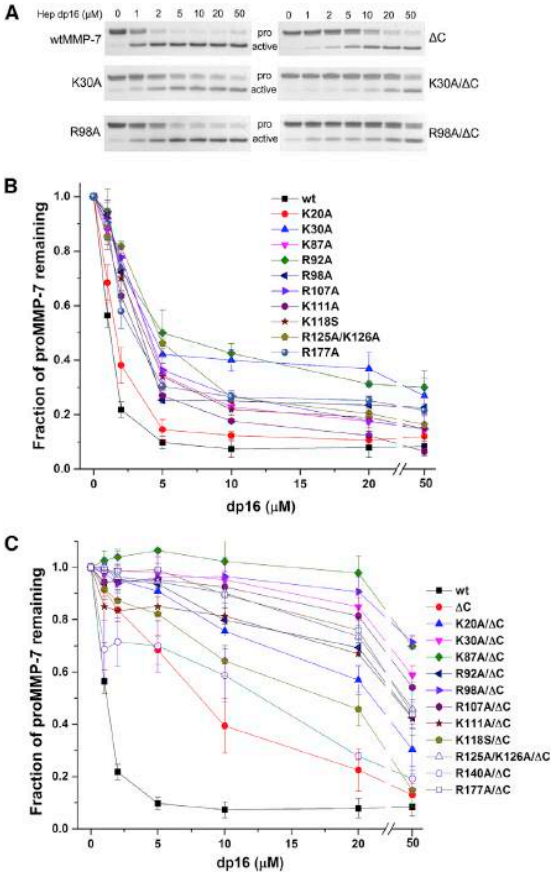

Figure 3. Dependence of Activation of proMMP-7 Mutants upon Heparin dp16

(A) The heparin dp16 dependence of the activation of proMMP-7 with wt sequence or a point mutation are compared, with or without the C-terminal peptide deletion. The incubations proceeded at 37°C for 2 hr with up to 50 μM heparin dp16.

(B) The portion of each unreacted variant of proMMP-7 remaining after the 2-hr incubation is plotted versus [heparin dp16]. The mean and SD of triplicate measurements are reported.

(C) The portion of each unreacted variant of proMMP-7ΔC is plotted.

See also Figure S4.

mutations upon activation, using heparin dp16 to trigger the removal of the pro-domain to form the mature protease (Fulcher et al., 2014) (Figure 3A). K30A, R92A, and R125A/K126A point mutations caused the most slowing of heparin dp16-induced activation (Figure 3B). K87A, R98A, R107A, K111A, K118S, and R177A also retarded the activation, but K20A only slightly (Figure 3B). Combining any of these ten point mutations with the removal of the C-terminal peptide dramatically decreased the activation triggered by heparin dp16 (Figure 3C). This indicates the importance of these ten sites for heparin binding that results in activation. The additivity between K118S and ΔC is less. Overall, the activation effects parallel the effects on binding detected by SPR.

There are exceptions to this general agreement. The K20A and K30A substitutions impaired activation more than binding (Figures 2 and 3). The R140A/ΔC combination disrupts much of the binding detected by SPR (Figure 2B), while scarcely impairing activation more than the ΔC lesion alone (Figure 3C).

The Reducing End of Heparin Is Close to Both Domains

We investigated the preferred orientations of binding of the heparin chain conjugated to a nitroxide spin label, which exerts paramagnetic broadening of the protein NMR resonances within about 22 Å of the unpaired electron. We conjugated TEMPO to the reducing end of heparin dp8 through reductive amination (Figure 4A). Mass spectral and NMR analyses indicated

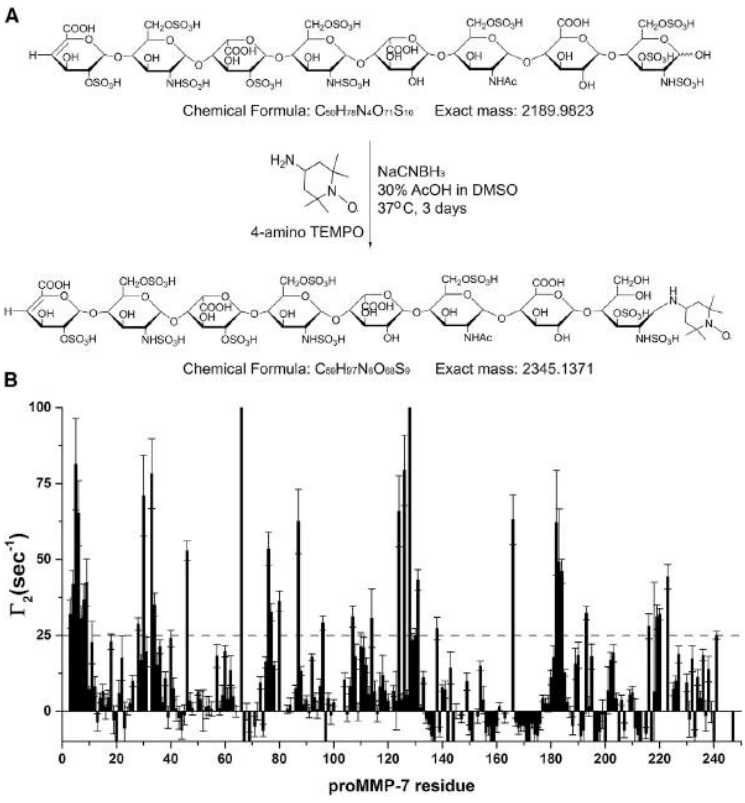

Figure 4. Spin Labeling of Heparin dp8 Suggests Close Approaches of the Reducing End to the Zymogen

(A) Nitroxide-containing TEMPO was coupled to heparin dp8 by reductive amination. See also Figures S5–S7.

(B) At 1.5-fold excess in a complex with proMMP-7(E195A) at 300 μM in physiological saline, this introduced the PREs plotted as Γ_2 relaxation rates, equaling $R_{2,para} - R_{2,dia}$. Residues with $\Gamma_2 > 25\ s^{-1}$ are considered as significant beyond the uncertainties. The error bars indicate the uncertainties in the exponential fits and propagation of the errors to the difference between paramagnetic and diamagnetic states.

conjugation of TEMPO to heparin dp8 in high yield (Figures S5–S7). We added the TEMPO-substituted heparin dp8 to 1.5-fold excess over proMMP-7(E195A) and measured the amide proton NMR relaxation of the paramagnetic mixture, as well as after ascorbate reduction of the nitroxide radical. We estimated the PREs as the differences between the ^{1}H NMR relaxation rate constants before and after reducing the nitroxide radical (Equation 3). In the pro-domain, two patches of residues have large PREs, indicating proximity to the spin label at the reducing end, i.e., to the backbone of Glu3 to Glu9 and Glu28, Lys30, Asn33, and Ser34 (Figure 4B). Gly5, Gly6, Lys30, and Asn33 exhibit PREs among the largest quantifiable ($\Gamma_2 > 65\ s^{-1}$) and occupy the center of these two surface patches (Figure 5C). These two patches are positioned on both rims of a shallow channel on the pro-domain (Figure 5C). Both surface patches agree with the chemical shift mapping (Figure 1). The patch of residues 28–34 agrees with the importance of Lys30 in heparin-triggered activation of the zymogen.

The TEMPO-substituted heparin dp8 introduced many PREs, significant beyond uncertainties, in the catalytic domain. PREs are observed at the exposed and scissile linker at Ser76 and Leu77, as well as Asn80 and Lys87 nearby (Figure 4B). A cluster of PREs are observed on the back of the catalytic domain at Asn114, Phe124, Lys126, and Val128 to Thr131 (Figures 4B and 5C). A looser group of PREs stretches from Phe138 and Tyr96 through Arg107 to Asn223. Also exhibiting PREs from the spin-labeled dp8 is a tight patch of residues outside one end of the active-site channel at Ser182 to Leu184 and Gly219 and Asp220. The arc of residues with PREs wrapping around the catalytic domain (Figure 5C) substantiates the hypothesis of such a swath on rat MMP-7 (Yu and Woessner, 2000). The spatial distribution of PREs suggests that heparin oligosaccharides visit at least two sites of binding.

4-mers Protect Similar Sites from a Gd·EDTA Probe

Prospective binding sites were also investigated by heparin dp4 protection of amide groups from solvent PREs introduced by Gd·EDTA (Arumugam et al., 1998; Madl et al., 2011). The pro-domain is very highly exposed and sensitive to large solvent PREs from Gd·EDTA. The most apparent protection of the surface by the tetrasaccharides is in the pro-domain (Figure 5B). Heparin dp4 significantly protected residues 3–6, 13, 16, 19, 30, 34, 37, 67, and 75 from Gd·EDTA, according to $\Delta\Gamma_2 > 40\ s^{-1}$ (Figures 5B and 5C). Residues 3–6 and 30 also exhibited proximity to the spin-labeled heparin dp8 (Figure 5C). Residues protected by heparin dp4 in the catalytic domain are fewer and circumscribe the β sheet: residues 86–88, 95, 124, 126, and 166 (Figures 5B and 5C). These are a subset of the residues affected by spin-labeled heparin dp8 (Figure 5C), consistent with dp4 binding with less affinity and fewer contacts with the catalytic domain than dp8.

8-mer Inserts in the Basic Pocket of Pro-domain and Reaches the Catalytic Domain

Calculations were performed to dock the heparin dp8 chain to the pro-domain of proMMP-7. The PREs of the protein amide groups from the spin-labeled heparin dp8 (Figure 4) provided explicit distance restraints that defined the location of the reducing end. These were supplemented by ambiguous distance restraints representing the heparin oligosaccharide

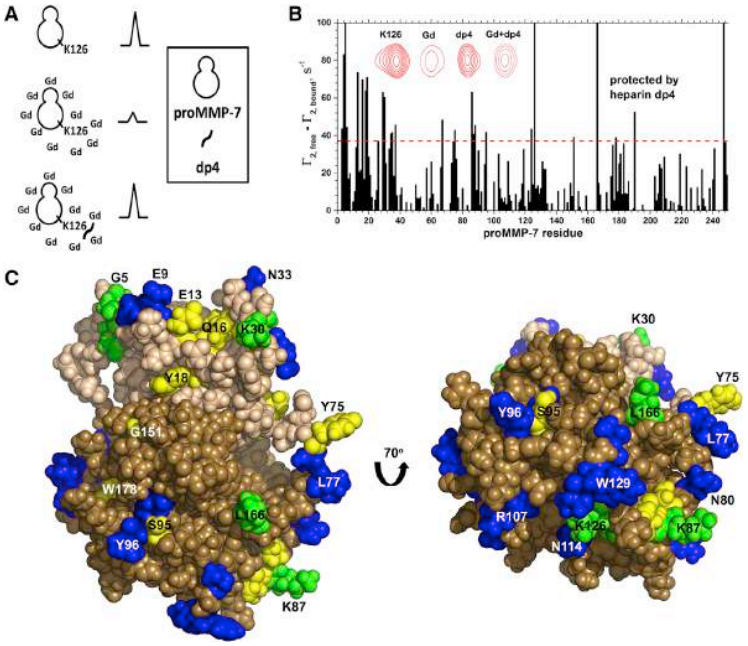

Figure 5. Heparin dp4 Protection of the Zymogen from NMR Line Broadening by Gd·EDTA

(A) This interface-mapping strategy measures the accessibility of the surface to Gd·EDTA as NMR line broadening, which is decreased by carbohydrate bound.

(B) PREs introduced by 0.3 mM Gd·EDTA to the free zymogen and its complexes with heparin dp4 are compared. The tetrasaccharide was added to 1.5-fold molar excess. The red contour lines in the inset compare NMR peaks of Lys126 in free and dp4-bound states, without and with Gd·EDTA. Decreases in $\Gamma_2 > 37\ s^{-1}$ once heparin dp4 was bound (above the dashed threshold) suggest greater protection of the surface by dp4.

(C) Paramagnetic mapping of proximity of heparin fragments is marked on the NMR structure of proMMP-7(E195A). Sites with large PREs introduced by spin-labeled heparin dp8 ($\Gamma_2 > 25\ s^{-1}$) are blue. Sites that heparin dp4 protects from broadening by Gd·EDTA ($\Delta\Gamma_2 > 37\ s^{-1}$) are yellow. Sites with both types of evidence of proximity to heparin oligosaccharides are green. The left panel includes binding patches on the pro-domain. The right panel shows the approaches of the heparin fragments to the catalytic domain.

contacts with the enzyme derived from exclusion of the Gd·EDTA probe, CSPs, and mutations interfering in maturation (Table 1). Representing the dynamic nature of heparin oligosaccharides, the pro-domain, and C terminus of proMMP-7 lay beyond the ability of rigid body docking that supports conformational flexibility only at interfaces. The torsion angle dynamics of CYANA, its reliance on explicit and ambiguous distance restraints (Guntert and Buchner, 2015), and the CYANA-calculated NMR structure of proMMP-7 (Prior et al., 2015) enabled us to compute models of glycan-proMMP-7 complexes with conformational diversity throughout the molecules consistent with the distance restraints. The resulting ensemble of 16 structural models most consistent with the restraints is defined similarly well as the NMR structure of the free state, except for an increased root-mean-square deviation (RMSD) of the N-terminal 20 residues and metal-binding S-shaped loop (Figure 6A). The structural ensemble strongly suggests that heparin dp8 extends from a basic pocket in the pro-domain past the S-shaped loop of the catalytic domain and on to an adjoining basic region (Figure 6B). The sulfated N-acetyl glucosamine of the reducing end, GlcNS6S 1, inserts into a pocket formed by Gln14, Asp17, Tyr18, Lys20, Arg21, Tyr25, and Lys30 (Figure 6C). The side chain of Arg21 makes favorable electrostatic contact with the 2-sulfate group of IdoA2S 2 in the majority of the structural models. Heparin residues IdoA2S 2 to GlcNS6S 5 approach Pro148, Phe149, Asp150, and Gly151 of the S-shaped loop (Figure 6C) in many of the structural models. The oligosaccharide chain continues along an electropositive path, passing near and between Arg140 and Arg177 (Figure 6B). The non-reducing end approaches the vicinity of Arg98, with increased exposure and RMSD (Figures 6A–6C). Thus, both domains each employ three basic residues to attract the oligosaccharide to span them.

Heparin dp8 Crosses the Remote Side of the Catalytic Domain and Meets the C Terminus

Docking to the catalytic domain proceeded via the same computational strategy but resulted in greater definition of the heparin octasaccharide (Figures 6A and 6D), due to more restraints based on mutations and a nuclear Overhauser effect (NOE) near the non-reducing end (Table 1 and Figure S2C). Heparin dp8 stretches along the long helix remote from the active site (Figure 6D). The reducing end of heparin dp8 is defined well by PREs emanating from its nitroxide spin label. GlcNS6S 1 fits into a basic channel with its sulfate groups in contact with the positive charges of the Arg125 and Lys247 side chains (Figure 6E). His123, Arg125, and Lys126 form one wall of the channel while Arg107, Lys111, Lys118, Arg245, Lys246, and Lys247 form the opposite wall. The latter three dynamic C-terminal residues appear to migrate considerably from their proximity to the pro-domain in the free state (PDB: 2mze); the C-terminal basic residues must be attracted to the heparin chain bound to the catalytic domain. IdoA2S 2 packs with Lys126 (Figure 6E). A sulfate group of GlcNS6S 3 is consistently close to the side chain of Arg107 (Figure 6E). A sulfate of GlcNS6S 5 is near the imidazole ring of His102 at the N terminus of the helix. The octasaccharide bends around the N-terminal end of the helix with its non-reducing end close to the side chain of Arg98 (Figures 6D and 6E), due to an NOE between a glycosidic proton and the amide group of Arg98 (Figure S2C). Thus, the arc of positive charge (Figure 2A) first recognized in the rat enzyme (Yu and Woessner, 2000) is indeed a principal binding site for heparinoids (Figure 6).

Table 1. Distance Restraints and Structural Statistics of Docking Heparin dp8 to the NMR Structure of Human proMMP7(E195A)

Type of Distance Restraint	Amide Groups Restrained in or Near Pro-domain	Amide Groups Restrained in Catalytic Domain
Paramagnetic relaxation enhancement[a]	E3, A4, G5, G6, M7, S8, E9, E28, K30, N33, S34, S76, L77	K87, Y96, R107, N114, F124, K126, V128, W129, R241
NOE	none	$R98H_N$ – GlcNS6S H1[b]
Mutation of Arg or Lys[c]	K20, K30, R177	K87, K111, K118, K126, K247, R92, R107, R125, R177, R245
Chemical shift perturbation[c]	Y25, N31, M62, D71	V89, L108, M115, H123
Protection from Gd·EDTA[c]	E3, A4, G5, G6, E13, Q16, Y18, L19, D26, T29, K30, S34, L35, A37, G151, W178	S86, K87, V88, S95, F124, K126, K247
RMSD of distance restraints (Å)	0.0123 ± 0.0004	0.013 ± 0.0012
Backbone RMSD to mean structure[d]	0.79 ± 0.11	0.65 ± 0.15
Heavy atom RMSD to mean structure[d]	1.40 ± 0.18	1.10 ± 0.19
Clashscore	2	1
PDB ID	5UE2	5UE5

[a]PRE-based distances are explicitly between the TEMPO spin label at the reducing end of heparin dp8 and the protein amide group.
[b]Restrained ambiguously to GlcNS6S 5 or 7.
[c]Restraints based on mutations, CSPs, or protection from Gd·EDTA are ambiguous in fostering proximity to any residue of heparin dp8.
[d]Across ordered enzyme residues 8–25, 33–72, 79–140, 151–216, 224–239, and heparin residues GlcNS6S1 to GlcNS6S7.

DISCUSSION

A Heparin-Binding Mode Conducive to Pericellular Proteolysis and Shedding

The path of binding across the back of the catalytic domain and C terminus (Figures 6C and 6D) enables a GAG chain long enough to link mature MMP-7 to GAG-associated substrates such as pro-α-defensin, pro-HB-EGF, syndecans-1, -2, and -4, or proMMP-7. HSPGs such as CD44 and the syndecans are key sources of bridging GAG chains (Yu and Woessner, 2000; Yu et al., 2002). Such bridging by GAG binding to the remote side of the catalytic domain should expedite proteolytic digestion by co-localization, without obstructing the catalytic cleft.

Maturation of MMP-7 and Potential Allosteric Roles

Activation of proMMP-7 by GAGs has been regarded as allosteric (Tocchi and Parks, 2013). Proteolytic removal of the pro-domain during maturation to the active enzyme is accelerated by heparin fragments and other GAGs (Ra et al., 2009), especially by those ≥16 residues long (Fulcher et al., 2014). The congregation of proMMP-7 molecules in elongated, irregular oligomers with the longer GAG chains is characteristic of maturation and may be the dominant consideration in the mechanism of maturation (Fulcher et al., 2014). Formation of these extended oligomers requires both the pro-domain and the basic C terminus (Fulcher et al., 2014). The two most probable modes of GAG binding to the pro-domain and C terminus have been elucidated (Figure 6). Additional, lesser modes of binding in which the spin-labeled reducing end of heparin dp8 approaches the patch of Ser182 to Leu184 and Asp220 and a looser patch of Leu77, Asn80, and Lys87 are suggested by PREs (Figures 4B and 5C). Together, the binding modes must facilitate many combinations of tandem and sandwiched orientations of the zymogens bound and bridged by GAG chains ≥16 residues long in the irregular oligomers.

Other structural aspects of the GAG binding may also foster the maturation. The mode of heparin binding bridging between domains (Figures 6B and 6C) could be conducive to activation of proMMP-7. The susceptibility of the pro-domain to proteolysis and its degree of exposure and disorder suggested by the solution structures probably facilitate its removal. The limited stability of the pro-domain is also suggested by K40S and K64A point mutations, rendering it more susceptible to proteolysis (see Figure S4). A GAG chain bridging between the domains might provide a means of mechanical pull or torque more likely to distort the pro-domain than the catalytic domain. GAG chains exceeding 12 residues in length should have higher affinity and probability of bridging between the domains. If the pro-domain is distorted or destabilized by the binding that bridges between domains, as suggested by bending of a helix at Gln16, the pro-domain may be more vulnerable to proteolytic removal for maturation. Also consistent with the hypothesis of distortion, the N-terminal 20 residues appear more disordered with heparin dp8 bound (Figures 6A and 6B).

Alternative means of allostery in GAG-triggered activation are possible. Cys67 coordination of the catalytic zinc is lost upon removal of the pro-domain during maturation. Heparin dp8-induced CSPs of Cys67 (Figure 1B) suggest its sensitivity to heparin fragments, despite its burial and distance from the binding sites. Bilayer binding to the back of the catalytic domain can disrupt Cys67 proximity to the zinc and trigger autolytic activation, potentially by the route of allosteric transmission proposed by Prior et al. (2015). The allosteric site where heparinoid binding triggers acceleration of the catalytic velocity of the mature enzyme (Fulcher et al., 2014) must be the heparin-binding site on the back of the catalytic domain (Figure 6C); this inference is based on this site and the allosteric enhancement of velocity remaining after deletion of the C-terminal basic peptide. The binding site for anionic lipid bilayers (Prior et al., 2015) and this heparin-binding site share the basic side chains of Arg98, His102, Arg107, Lys111, Lys118, Arg125, and Lys126 (Figure 6D). As the C terminus also appears to contribute to this allosteric site (Figure 6D) and deletion of the C-terminal octapeptide decreases allosteric enhancement of velocity (Fulcher et al.,

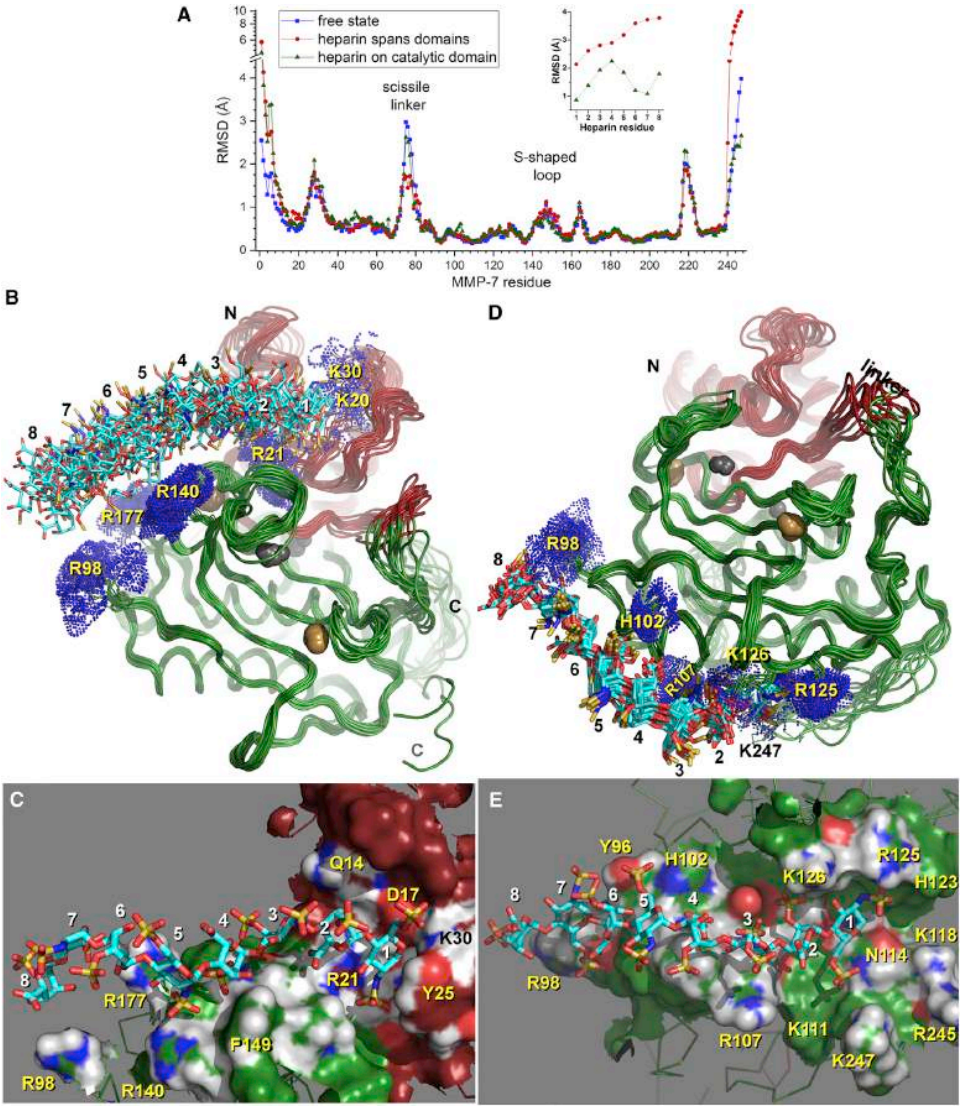

Figure 6. Heparin dp8 Bound to Two Basic Tracks on proMMP-7

(A) Average backbone RMSD values to the mean are plotted for the structural ensembles of the free state (PDB: 2MZE), the complex with heparin dp8 bridging between domains (PDB: 5UE2), and the complex with the octasaccharide bound to the catalytic domain (PDB: 5UE5). The inset plots the average RMSD to the mean for carbohydrate atoms C1 to C4, O4, and O5.

(B) The octasaccharide spans between the domains in the 16 members of the ensemble. The pro-domain is colored red and the catalytic domain green. Side-chain nitrogen atoms of interfacial side chains are plotted with dots. Atoms are color-coded red for oxygen, blue for nitrogen, yellow for sulfur, white for hydrogen, gray for zinc, tan for calcium, gray for zinc, cyan for carbon in dp8, red for carbon in the pro-domain, and green for carbon in the catalytic domain. Sulfate oxygens and O3 are omitted from the structural ensembles for clarity.

(C) Low-energy model 1 of the interdomain binding mode plots heparin dp8 with all atoms and the protease with sticks and a molecular surface colored by atom type at the interface.

(D) The mode of heparin dp8 binding on the distal face of the catalytic domain is plotted for all 16 members of the ensemble.

(E) Low-energy model 1 of the complex with heparin dp8 bound on the back of the catalytic domain is plotted with a surface at the interface.

2014), the C-terminal peptide may contribute to the allosteric transmission, possibly by its reorienting to join the GAG-binding site on the back of the catalytic domain as implied by PREs (compare Figures 6B and 6D).

Capture of Heparin Oligosaccharides by Charge

Of the structural features of proMMP-7 recognizing heparin oligosaccharides, the charge complementarity looms largest. The reducing end at both binding sites is surrounded by at least three basic side chains: Lys20, Arg21, and Lys30 or Arg125, Lys126, Arg245, and Lys247 (Figure 6). The insertion of the reducing end into these basic pockets may be attributable to the greater negative charge density on GlcNS6S 1 than on IdoA2S 8 of the non-reducing end. This supplements the evidence from NMR, mutagenesis, and salt-dependent affinity that complementary charge dominates in the association of heparinoid chains with proMMP-7. The middle of the heparin dp8 bound to the catalytic domain appears attracted to Arg107 and His102, while the non-reducing end is near Arg98 (Figure 6D). The middle of the octasaccharide bridging between domains seems attracted to both Arg140 and Arg177, and the non-reducing end to Arg98 (Figure 6). The convergence of the two binding paths near Arg98 suggests the possibility of the two binding strips being joined into a single trajectory that a longer GAG chain may bind.

Electrostatically guided heparinoid interactions with proMMP-7 are emerging as a relatively well-characterized and complex case study with parallels to the GAG binding and activation of certain other proteases. Electrostatic association of GAGs with those proteases triggering release of the pro-domain is likely to be a unifying concept among the disparate types of proteases. The precedent of a protease binding GAG chains along basic strips in a complex, oligomeric manner that triggers proteolytic activity was established thoroughly for cathepsin K (Cherney et al., 2011; Li et al., 2008; Nallaseth et al., 2013). The GAG interactions of a diversity of GAG-binding proteins have been characterized (Capila and Linhardt, 2002; Xu and Esko, 2014). Most proteins bind GAGs on their surfaces primarily through electrostatics and do not undergo conformational changes. The micromolar K_D values of heparin dp8 for proMMP-7 (Figures 1 and S3) rank among the cases of lower affinity and specificity when compared with a recent survey (Xu and Esko, 2014). Nonetheless, there is large pathophysiological impact of GAG-induced activation of proMMP-7 (Rohani and Parks, 2015; Tocchi and Parks, 2013) and shedding of key proteins from cell surfaces (Li et al., 2002; Ryu et al., 2009; Wilson et al., 1999; Yu et al., 2002). Heparin dp8 may enhance disorder near the N terminus (Figure 6A) and appears to recruit the basic and dynamic C terminus a significant distance to the binding site on the back of the catalytic domain (Figure 6D), perhaps facilitating maturation (Figure 3). The potential for heparin to induce large conformational changes was already established by crystallographic characterization of the heparin activation of the serine protease inhibitor antithrombin (Johnson et al., 2006).

STAR★METHODS

Detailed methods are provided in the online version of this paper and include the following:

ACCESSION NUMBERS

The solution structural coordinates of proMMP-7 complexes with heparin octasaccharides are deposited under RCSB PDB accession codes PDB: 5UE2 and 5UE5.

SUPPLEMENTAL INFORMATION

Supplemental Information includes seven figures and two data files and can be found with this article online at http://dx.doi.org/10.1016/j.str.2017.05.019.

AUTHOR CONTRIBUTIONS

Conceptualization, S.R.v.D. and R.J.L.; Methodology, S.R.v.D., Y.G.F., S.H.P., R.J.L., and F.Z.; Investigation, Y.G.F., F.Z., S.H.P., and S.R.v.D.; Resources, Y.G.F., S.M., L.L., D.P., and R.J.L.; Software, S.H.P.; Validation, S.R.v.D.; Data Curation, S.R.v.D.; Writing – Original Draft, S.R.v.D. and Y.G.F.; Writing – Review and Editing, F.Z., S.H.P., R.J.L., and S.R.v.D.; Visualization, Y.G.F., F.Z., and S.R.v.D.; Funding Acquisition, S.R.v.D., R.J.L., and F.Z.

ACKNOWLEDGMENTS

We thank William C. Parks for inspiring investigation of this topic. This work was supported by NIH grant R01 GM057289. The 800 MHz NMR spectrometer and cryoprobe were purchased with funds from the University of Missouri and NIH grant S10 RR022341.

Received: December 30, 2016
Revised: April 14, 2017
Accepted: May 24, 2017
Published: June 22, 2017

REFERENCES

Arumugam, S., Hemme, C.L., Yoshida, N., Suzuki, K., Nagase, H., Berjanskii, M., Wu, B., and Van Doren, S.R. (1998). TIMP-1 contact sites and perturbations of stromelysin 1 mapped by NMR and a paramagnetic surface probe. Biochemistry *37*, 9650–9657.

Battiste, J.L., and Wagner, G. (2000). Utilization of site-directed spin labeling and high-resolution heteronuclear nuclear magnetic resonance for global fold determination of large proteins with limited nuclear overhauser effect data. Biochemistry *39*, 5355–5365.

Capila, I., and Linhardt, R.J. (2002). Heparin-protein interactions. Angew. Chem. Int. Ed. *41*, 391–412.

Chen, P., Abacherli, L.E., Nadler, S.T., Wang, Y., Li, Q., and Parks, W.C. (2009). MMP7 shedding of syndecan-1 facilitates re-epithelialization by affecting alpha(2)beta(1) integrin activation. PLoS One *4*, e6565.

Cherney, M.M., Lecaille, F., Kienitz, M., Nallaseth, F.S., Li, Z., James, M.N., and Bromme, D. (2011). Structure-activity analysis of cathepsin K/chondroitin 4-sulfate interactions. J. Biol. Chem. *286*, 8988–8998.

Choi, S., Kim, J.-Y., Park, J.H., Lee, S.-T., Han, I.-O., and Oh, E.-S. (2012). The matrix metalloproteinase-7 regulates the extracellular shedding of syndecan-2 from colon cancer cells. Biochem. Biophys. Res. Commun. *417*, 1260–1264.

Clore, G.M. (2015). Chapter 17. Practical aspects of paramagnetic relaxation enhancement in biological macromolecules. In Methods in Enzymology, Z.Q. Peter and W. Kurt, eds. (Academic Press), pp. 485–497.

Conrad, H.E. (1998). Heparin-Binding Proteins (Academic Press).

Crabbe, T., Ioannou, C., and Docherty, A.J. (1993). Human progelatinase A can be activated by autolysis at a rate that is concentration-dependent and enhanced by heparin bound to the C-terminal domain. Eur. J. Biochem. *218*, 431–438.

DeLano, W.L. (2002). The PyMOL Molecular Graphics System (DeLano Scientific).

Fingleton, B.M., Heppner Goss, K.J., Crawford, H.C., and Matrisian, L.M. (1999). Matrilysin in early stage intestinal tumorigenesis. APMIS *107*, 102–110.

Fulcher, Y.G., Sanganna Gari, R.R., Frey, N.C., Zhang, F., Linhardt, R.J., King, G.M., and Van Doren, S.R. (2014). Heparinoids activate a protease, secreted by mucosa and tumors, via tethering supplemented by allostery. ACS Chem. Biol. *9*, 957–966.

Garimella, R., Liu, X., Qiao, W., Liang, X., Zuiderweg, E.R., Riley, M.I., and Van Doren, S.R. (2006). Hsc70 contacts helix III of the J domain from polyomavirus T antigens: addressing a dilemma in the chaperone hypothesis of how they release E2F from pRb. Biochemistry *45*, 6917–6929.

Gill, S.E., and Parks, W.C. (2008). Metalloproteinases and their inhibitors: regulators of wound healing. Int. J. Biochem. Cell Biol. *40*, 1334–1347.

Gill, S.E., Nadler, S.T., Li, Q., Frevert, C.W., Park, P.W., Chen, P., and Parks, W.C. (2016). Shedding of syndecan-1/CXCL1 complexes by matrix metalloproteinase 7 functions as an epithelial checkpoint of neutrophil activation. Am. J. Respir. Cell Mol. Biol. *55*, 243–251.

Goddard, T.D., and Kneller, D.G. (2000). SPARKY (University of California, San Francisco).

Guntert, P., and Buchner, L. (2015). Combined automated NOE assignment and structure calculation with CYANA. J. Biomol. NMR *62*, 453–471.

Hartmann-Petersen, S., Tammi, R.H., Tammi, M.I., and Kosma, V.M. (2009). Depletion of cell surface CD44 in nonmelanoma skin tumours is associated with increased expression of matrix metalloproteinase 7. Br. J. Dermatol. *160*, 1251–1257.

Hayashida, K., Parks, W.C., and Park, P.W. (2009). Syndecan-1 shedding facilitates the resolution of neutrophilic inflammation by removing sequestered CXC chemokines. Blood *114*, 3033–3043.

Humphrey, W., Dalke, A., and Schulten, K. (1996). VMD: visual molecular dynamics. J. Mol. Graph. *14*, 33–38, 27-8.

Iida, J., Wilhelmson, K.L., Ng, J., Lee, P., Morrison, C., Tam, E., Overall, C.M., and McCarthy, J.B. (2007). Cell surface chondroitin sulfate glycosaminoglycan in melanoma: role in the activation of pro-MMP-2 (pro-gelatinase A). Biochem. J. *403*, 553–563.

Iwahara, J., Tang, C., and Marius Clore, G. (2007). Practical aspects of (1)H transverse paramagnetic relaxation enhancement measurements on macromolecules. J. Magn. Reson. *184*, 185–195.

Johnson, D.J., Li, W., Adams, T.E., and Huntington, J.A. (2006). Antithrombin-S195A factor Xa-heparin structure reveals the allosteric mechanism of antithrombin activation. EMBO J. *25*, 2029–2037.

Kailemia, M.J., Li, L., Ly, M., Linhardt, R.J., and Amster, I.J. (2012). Complete mass spectral characterization of a synthetic ultralow-molecular-weight heparin using collision-induced dissociation. Anal. Chem. *84*, 5475–5478.

Khan, S., Gor, J., Mulloy, B., and Perkins, S.J. (2010). Semi-rigid solution structures of heparin by constrained x-ray scattering modelling: new insight into heparin–protein complexes. J. Mol. Biol. *395*, 504–521.

Koppisetti, R.K., Fulcher, Y.G., Jurkevich, A., Prior, S.H., Xu, J., Lenoir, M., Overduin, M., and Van Doren, S.R. (2014). Ambidextrous binding of cell and membrane bilayers by soluble matrix metalloproteinase-12. Nat. Commun. *5*, 5552.

Koradi, R., Billeter, M., and Wuthrich, K. (1996). MOLMOL: a program for display and analysis of macromolecular structures. J. Mol. Graph. *14*, 51–55, 29-32.

Lang, R., Kocourek, A., Braun, M., Tschesche, H., Huber, R., Bode, W., and Maskos, K. (2001). Substrate specificity determinants of human macrophage elastase (MMP-12) based on the 1.1 A crystal structure. J. Mol. Biol. *312*, 731–742.

Lee, D., Hilty, C., Wider, G., and Wuthrich, K. (2006). Effective rotational correlation times of proteins from NMR relaxation interference. J. Magn. Reson. *178*, 72–76.

Lescop, E., Kern, T., and Brutscher, B. (2010). Guidelines for the use of band-selective radiofrequency pulses in hetero-nuclear NMR: example of longitudinal-relaxation-enhanced BEST-type 1H-^{15}N correlation experiments. J. Magn. Reson. *203*, 190–198.

Li, Q., Park, P.W., Wilson, C.L., and Parks, W.C. (2002). Matrilysin shedding of syndecan-1 regulates chemokine mobilization and transepithelial efflux of neutrophils in acute lung injury. Cell *111*, 635–646.

Li, Z., Kienetz, M., Cherney, M.M., James, M.N., and Bromme, D. (2008). The crystal and molecular structures of a cathepsin K:chondroitin sulfate complex. J. Mol. Biol. *383*, 78–91.

Liu, Y., and Prestegard, J.H. (2008). Direct measurement of dipole-dipole/CSA cross-correlated relaxation by a constant-time experiment. J. Magn. Reson. *193*, 23–31.

Lynch, C.C., Vargo-Gogola, T., Martin, M.D., Fingleton, B., Crawford, H.C., and Matrisian, L.M. (2007). Matrix metalloproteinase 7 mediates mammary epithelial cell tumorigenesis through the ErbB4 receptor. Cancer Res. *67*, 6760–6767.

Madl, T., Guttler, T., Gorlich, D., and Sattler, M. (2011). Structural analysis of large protein complexes using solvent paramagnetic relaxation enhancements. Angew. Chem. Int. Ed. *50*, 3993–3997.

Malde, A.K., Zuo, L., Breeze, M., Stroet, M., Poger, D., Nair, P.C., Oostenbrink, C., and Mark, A.E. (2011). An automated force field topology builder (ATB) and repository: version 1.0. J. Chem. Theory Comput. *7*, 4026–4037.

Malla, N., Berg, E., Theocharis, A.D., Svineng, G., Uhlin-Hansen, L., and Winberg, J.O. (2013). In vitro reconstitution of complexes between pro-matrix metalloproteinase-9 and the proteoglycans serglycin and versican. FEBS J. *280*, 2870–2887.

Marcink, T.C., Koppisetti, R.K., Fulcher, Y.G., and Van Doren, S.R. (2017). Mapping lipid bilayer recognition sites of metalloproteinases and other prospective peripheral membrane proteins. In Matrix Metalloproteases: Methods and Protocols, C.A. Galea, ed. (Springer New York), pp. 61–86.

Mitsiades, N., Yu, W.H., Poulaki, V., Tsokos, M., and Stamenkovic, I. (2001). Matrix metalloproteinase-7-mediated cleavage of Fas ligand protects tumor cells from chemotherapeutic drug cytotoxicity. Cancer Res. *61*, 577–581.

Muñoz, E.M., and Linhardt, R.J. (2004). Heparin-binding domains in vascular biology. Arterioscler. Thromb. Vasc. Biol. *24*, 1549–1557.

Nallaseth, F.S., Lecaille, F., Li, Z., and Bromme, D. (2013). The role of basic amino acid surface clusters on the collagenase activity of cathepsin K. Biochemistry *52*, 7742–7752.

Ori, A., Wilkinson, M.C., and Fernig, D.G. (2011). A systems biology approach for the investigation of the heparin/heparan sulfate interactome. J. Biol. Chem. *286*, 19892–19904.

Parks, W.C., Lopez-Boado, Y.S., and Wilson, C.L. (2001). Matrilysin in epithelial repair and defense. Chest *120*, 36S–41S.

Pervin, A., Gallo, C., Jandik, K.A., Han, X.J., and Linhardt, R.J. (1995). Preparation and structural characterization of large heparin-derived oligosaccharides. Glycobiology *5*, 83–95.

Prior, S.H., Fulcher, Y.G., Koppisetti, R.K., Jurkevich, A., and Van Doren, S.R. (2015). Charge-triggered membrane insertion of matrix Metalloproteinase-7, supporter of innate immunity and tumors. Structure *23*, 2099–2110.

Ra, H.J., Harju-Baker, S., Zhang, F., Linhardt, R.J., Wilson, C.L., and Parks, W.C. (2009). Control of promatrilysin (MMP7) activation and substrate-specific activity by sulfated glycosaminoglycans. J. Biol. Chem. *284*, 27924–27932.

Rohani, M.G., and Parks, W.C. (2015). Matrix remodeling by MMPs during wound repair. Matrix Biol. *44-46*, 113–121.

Ryu, H.-Y., Lee, J., Yang, S., Park, H., Choi, S., Jung, K.-C., Lee, S.-T., Seong, J.-K., Han, I.-O., and Oh, E.-S. (2009). Syndecan-2 functions as a docking receptor for pro-matrix Metalloproteinase-7 in human colon cancer cells. J. Biol. Chem. *284*, 35692–35701.

Sakurai, K., and Goto, Y. (2007). Principal component analysis of the pH-dependent conformational transitions of bovine beta-lactoglobulin monitored by heteronuclear NMR. Proc. Natl. Acad. Sci. USA *104*, 15346–15351.

Studier, F.W. (2005). Protein production by auto-induction in high density shaking cultures. Protein Expr. Purif. *41*, 207–234.

Theocharis, A.D., Gialeli, C., Bouris, P., Giannopoulou, E., Skandalis, S.S., Aletras, A.J., Iozzo, R.V., and Karamanos, N.K. (2014). Cell-matrix interactions: focus on proteoglycan-proteinase interplay and pharmacological targeting in cancer. FEBS J. *281*, 5023–5042.

Tocchi, A., and Parks, W.C. (2013). Functional interactions between matrix metalloproteinases and glycosaminoglycans. FEBS J. *280*, 2332–2341.

Vargo-Gogola, T., Fingleton, B., Crawford, H.C., and Matrisian, L.M. (2002). Matrilysin (matrix metalloproteinase-7) selects for apoptosis-resistant mammary cells in vivo. Cancer Res. *62*, 5559–5563.

Wells, J.A. (1990). Additivity of mutational effects in proteins. Biochemistry *29*, 8509–8517.

Wilson, C.L., Ouellette, A.J., Satchell, D.P., Ayabe, T., Lopez-Boado, Y.S., Stratman, J.L., Hultgren, S.J., Matrisian, L.M., and Parks, W.C. (1999). Regulation of intestinal alpha-defensin activation by the metalloproteinase matrilysin in innate host defense. Science *286*, 113–117.

Xu, D., and Esko, J.D. (2014). Demystifying heparan sulfate-protein interactions. Annu. Rev. Biochem. *83*, 129–157.

Xu, J., and Van Doren, S.R. (2016). Binding isotherms and time courses readily from magnetic resonance. Anal. Chem. *88*, 8172–8178.

Xu, J., and Van Doren, S.R. (2017). Tracking equilibrium and nonequilibrium shifts in data with TREND. Biophys. J. *112*, 224–233.

Yu, W.H., and Woessner, J.F., Jr. (2000). Heparan sulfate proteoglycans as extracellular docking molecules for matrilysin (matrix metalloproteinase 7). J. Biol. Chem. *275*, 4183–4191.

Yu, W.H., Woessner, J.F., Jr., McNeish, J.D., and Stamenkovic, I. (2002). CD44 anchors the assembly of matrilysin/MMP-7 with heparin-binding epidermal growth factor precursor and ErbB4 and regulates female reproductive organ remodeling. Genes Dev. *16*, 307–323.

Zhang, F., Zhang, Z., Lin, X., Beenken, A., Eliseenkova, A.V., Mohammadi, M., and Linhardt, R.J. (2009). Compositional analysis of heparin/heparan sulfate interacting with fibroblast growth factor.fibroblast growth factor receptor complexes. Biochemistry *48*, 8379–8386.

Zhang, L., Yang, M., Yang, D., Cavey, G., Davidson, P., and Gibson, G. (2010). Molecular interactions of MMP-13 C-terminal domain with chondrocyte proteins. Connect. Tissue Res. *51*, 230–239.

Zheng, X., Ou, L., Tong, X., Zhu, J., and Wu, H. (2007). Over-expression and refolding of isotopically labeled recombinant catalytic domain of human macrophage elastase (MMP-12) for NMR studies. Protein Expr. Purif. *56*, 160–166.

STAR★METHODS

KEY RESOURCES TABLE

REAGENT or RESOURCE	SOURCE	IDENTIFIER
Chemicals, Peptides, and Recombinant Proteins / DNA		
wt proMMP-7	Fulcher et al., 2014	pWT
proMMP-7(E195A)	Fulcher et al., 2014	pE195A
proMMP-7ΔC	Fulcher et al., 2014	pΔC
proMMP-7(K20A)	This work	pK20A
proMMP-7ΔC(K20A)	This work	pK20AΔC
proMMP-7(K20A/E195A)	This work	pK20AE195A
proMMP-7(K30A)	This work	pK30A
proMMP-7ΔC(K30A)	This work	pK30AΔC
proMMP-7(K30A/E195A)	This work	pK30AE195A
proMMP-7ΔC(K40S)	This work	pK40SΔC
proMMP-7ΔC(K64A)	This work	pK64AΔC
proMMP-7(K87A)	This work	pK87A
proMMP-7ΔC(K87A)	This work	pK87AΔC
proMMP-7(K87A/E195A)	This work	pK87AE195A
proMMP-7(R92A)	This work	pR92A
proMMP-7ΔC(R92A)	This work	pR92AΔC
proMMP-7(R92A/E195A)	This work	pR92AE195A
proMMP-7(R98A)	This work	pR98A
proMMP-7ΔC(R98A)	This work	pR98AΔC
proMMP-7(R98A/E195A)	This work	pR98AE195A
proMMP-7(R107A)	This work	pR107A
proMMP-7ΔC(R107A)	This work	pR107AΔC
proMMP-7(R107A/E195A)	This work	pR107AE195A
proMMP-7(K111A)	This work	pK111A
proMMP-7ΔC(K111A)	This work	pK111AΔC
proMMP-7(K111A/E195A)	This work	pK111AE195A
proMMP-7(K118A)	This work	pK118A
proMMP-7ΔC(K118A)	This work	pK118AΔC
proMMP-7(K118A/E195A)	This work	pK118AE195A
proMMP-7ΔC(H123A)	This work	pH123AΔC
proMMP-7(R125A/K126A)	This work	pRK125-6AA
proMMP-7ΔC(R125A/ K126A)	This work	pRK125-6AAΔC
proMMP-7(R125A/K126A /E195A)	This work	pRK125-6AAE195A
proMMP-7ΔC(R140A)	This work	pR140AΔC
proMMP-7(R177A)	This work	pR177A
proMMP-7ΔC(R177A)	This work	pR177AΔC
proMMP-7(R177A/E195A)	This work	pR177AE195A
PCR master mix	Agilent	600870
Kanamycin sulfate	Fisher	BP906-5
IPTG	Research Products International	I56000-5.0
EDTA	Fisher	BP118-500
HEPES	Fisher	BB310-1
Acetic acid	Fisher	A385-212
Urea	Fisher	U15-3

(*Continued on next page*)

Continued

REAGENT or RESOURCE	SOURCE	IDENTIFIER
$CaCl_2$	Fisher	C79-500
NaCl	Fisher	S271-50
ZnCl	Fisher	Z31-3
2-mercaptoethanol	Acros Organics	125472500
NaN_3	Fisher	BP922-500
D_2O, 99.8 atom%	Sigma-Aldrich	756822-1.107KG
$^{15}NH_4Cl$	Sigma-Aldrich	299251-10G
Imidazole	Fisher	O3196-500
Gd(III)Cl	Sigma	G-7532
bovine lung heparin	Sigma-Aldrich	H4898
Heparin lyase I	Heparin lyase I (EC # 4.2.2.7) was produced from recombinant *E. coli* in Linhardt laboratory.	N/A
Surfactant P20	GE Healthcare	BR100054
Brij-35	Acros Organics	329581000
Triton X-100	Fisher	BP151-100
Critical Commercial Assays		
T7 Primer for sequencing: TAATACGACTCACTATAGGG	IDT	N/A
SP Sepharose Fast Flow	GE Healthcare, Sigma-Aldrich	Sigma S1799
Porcine intestinal heparin (16 kD)	Celsus, Cincinatti	PH-91816
Streptavidin chip for Biacore	GE Healthcare	BR-1003-98
Deposited Data		
Coordinates, human proMMP-7 with heparin dp8 at pro-domain	This paper	PDB: 5UE2
Coordinates, proMMP-7 with heparin dp8 at catalytic domain	This paper	PDB: 5UE5
Coordinates of free state of proMMP-7	Prior et al., 2015	PDB: 2MZE
NMR peak assignments of free state	Prior et al., 2015	BMRB: 25485
Software and Algorithms		
Topspin 3.2 for NMR acquisition and processing	Bruker	https://www.bruker.com/nc/service/support-upgrades/software-downloads/nmr/free-topspin-processing/free-topspin-download.html
Sparky for NMR spectra	Goddard and Kneller, 2000	http://www.nmrfam.wisc.edu/nmrfam-sparky-distribution.htm
Principal component analysis	MATLAB	Statistics Toolbox
TREND for binding isotherms from spectra	Xu and Van Doren, 2017	http://biochem.missouri.edu/trend/
Automated Topology Builder	Malde et al., 2011	https://atb.uq.edu.au/
CYANA 2.1	Guntert and Buchner, 2015	http://enmr.chemie.uni-frankfurt.de/portal/cyana.html
Sybyl X 2.1.1	Certara	https://www.certara.com/software/molecular-modeling-and-simulation/sybyl-x-suite/
Molmol	Koradi et al., 1996	https://sourceforge.net/projects/molmol/
Pymol	DeLano, 2002	https://www.pymol.org/
VMD	Humphrey et al., 1996	http://www.ks.uiuc.edu/Research/vmd/
BIAevaluation 4.0.1	GE Healthcare	https://www.biacore.com/lifesciences/service/downloads/software_licenses/biaevaluation/
BIAcore control software 4.0.1	GE Healthcare	https://www.biacore.com/lifesciences/service/downloads/downloads/index.html

CONTACT FOR REAGENT AND RESOURCE SHARING

Further information and requests for resources and reagents should be directed to and will be fulfilled by the Lead Contact, Steven R. Van Doren (vandorens@missouri.edu).

EXPERIMENTAL MODEL AND SUBJECT DETAILS

Recombinant human proMMP-7 and variants were expressed in *E. coli* strain BL21 CodonPlus (DE3)-RIPL (Agilent Technologies).

METHOD DETAILS

Preparation of proMMP-7 Zymogen

The coding frame for human proMMP-7 was synthesized with codons optimized for *E. coli* by GenScript and subcloned into pET27b(+) (Novagen) (Fulcher et al., 2014). For assays by NMR and surface plasmon resonance (SPR), each of the pro-enzyme variants carried the inactivating E195A mutation in the active site to prevent *trans*-activation. Glu195 was retained intact for the *trans*-activation studies. Mutations were constructed by the QuickChange approach using PCR master mix (Agilent). For activation and SPR assays, the proMMP-7 variants were expressed in Luria broth. Kanamycin (100 μg/ml) in the growth medium selected for the expression vector. For NMR, proMMP-7(E195A) was expressed in PG minimal medium using D-glucose as the carbon source, $^{15}NH_4Cl$ as the nitrogen source, trace metals (Studier, 2005), and D_2O as the solvent. Protein expression was induced in the *E. coli* BL21 CodonPlus (DE3)-RIPL host strain (Agilent) in early log phase using 0.5 mM IPTG. The bacterial cell pellet harvested by centrifugation was suspended to homogeneity using a motor-driven Potter-Elvehjem tissue grinder and broken by sonication in 20 mM Tris·HCl (pH 7.5), 10 mM EDTA. The inclusion bodies harvested by centrifugation at 20,000 x g for 40 min. at 4°C and washed with 20 mM Tris·HCl (pH 7.5) containing 0.01% Triton-X 100 (Marcink et al., 2017). The inclusion bodies were dissolved with 6 M urea, 20 mM Tris·acetate (pH 4.5) and loaded onto a SP-Sepharose Fast Flow column equilibrated with 6 M urea in 20 mM Tris·acetate (pH 4.5). ProMMP-7 was eluted with a 0 to 1 M NaCl gradient and its fractions pooled and diluted to 0.1 mg/ml protein in refolding buffer of 10 mM HEPES·KOH (pH 7.5), 10 mM $CaCl_2$, 10 mM 2-mercaptoethanol with 6 M urea. For refolding, this was dialyzed in steps against 20 volumes of refolding buffer containing 3 M urea for 4 h, followed by 1 M urea overnight, then 0 M urea for 3 hr, and finally 0.1 mM $ZnCl_2$ for 1 h (Zheng et al., 2007). A final step of ion exchange chromatography used SP-Sepharose Fast Flow with column buffer of 10 mM HEPES-KOH (pH 7.5), 10 mM $CaCl_2$, 10 mM 2-mercaptoethanol, and 0.1 mM $ZnCl_2$ with a gradient of 0 to 1 M NaCl (Fulcher et al., 2014). The proMMP-7 was pooled with glycerol added to 50% (w/v) and frozen in aliquots at -80°C.

Preparation and Characterization of Heparin Oligosaccharides

Heparin dp4, dp8 and dp16 were prepared from commercial porcine intestinal heparin (Celsus Laboratories, Cincinnati, OH) by enzymatic digestion as described previously (Pervin et al., 1995). Briefly, heparin was partially digested by heparinase I (EC 4.2.2.7) at 30°C and the reaction was quenched in a 100°C water bath for 10 min when it reached 30% digestion as determined by ultraviolet absorbance. The reaction mixture was concentrated and size fractionated on a P-10 Biogel (BioRad, Hercules, CA) column (1.5 m × 5 cm) eluting with 0.2 M NaCl solution and detecting at 232 nm. Pooled oligosaccharide mixtures of different sizes were desalted on a P-2 column. The lyophilized uniform-sized oligosaccharide mixtures were purified on a semi-preparative SAX-HPLC (Shimadzu, Kyoto, Japan) column. The column was loaded with 1.25 mg of the uniform-sized oligosaccharide mixture and fractions were combined from repeated separations based on their retention time and chromatographic profiles as detected at 232 nm. The last major peak in each chromatogram, corresponding to the major trisulfated disaccharide repeating unit of heparin were collected (Figure S1) and characterized by MS (Figure S5) and NMR (Figure S6).

Heparin dp8 (1.5 mg, 0.68 μmol) was dissolved in 30% acetic acid in dimethylsulfoxide (1.1 mL). The 4-amino-TEMPO spin label (SL) (56.4 mg, 329 μmol) and sodium cyanoborohydride (69.1 mg, 1.1 mmol) were added to the solution and the reaction mixture was stirred at 37°C for 3 days. The reaction was then diluted with water and desalted by loading onto pre-rinsed 3000 molecular weight cutoff Amicon ultra (Millipore) spin column. The supernatant containing the SL heparin dp8 was collected and loaded onto the spin column for a second time. The supernatant was collected and lyophilized, affording SL-dp8 (1.1 mg, 0.47 μmol).

The structure of heparin dp8 and SL heparin dp8 were determined by nanospray LTQ-Orbitrap XL Fourier transform (FT) mass spectrometry (MS) and tandem MS (Thermo Fisher Scientific, San-Jose, CA) using conditions described previously (Kailemia et al., 2012) (Figures S5 and S6). The structures of heparin dp8 and SL heparin dp8 were next determined by ^{1}H-NMR analysis. The oligosaccharide was dissolved in 400 μL deuterium oxide (99.9 %, Sigma-Aldrich, St. Louis, MO) and lyophilized three times to remove the exchangeable protons. The samples were re-dissolved in 400 μL deuterium oxide and transferred to NMR microtubes. All NMR experiments were performed at 298 K on Bruker Advance II 600 MHz with Topspin 2.1.6 software. One-dimensional ^{1}H spectra were recorded (Figure S7).

NMR of Heparin dp8 Binding Sites and Affinity

NMR spectra of proMMP-7 (E195A) were collected at 37°C in 20 mM imidazole (pH 6.6),140 mM NaCl, 10 mM $CaCl_2$, 20 μM $ZnCl_2$, 10 mM 2-mercaptoethanol (Prior et al., 2015) and 7% D_2O using a Bruker 800 MHz Avance III spectrometer with TCI cryoprobe. NMR

spectra were acquired and processed with Bruker Topspin and interpreted using Sparky (Goddard and Kneller, 2000). Chemical shift perturbations of backbone amide ^{1}H and ^{15}N frequencies were monitored using Best-TROSY spectra (Lescop et al., 2010) with additions of heparin dp8 up to 1.5-fold molar excess over the 300 μM pro-enzyme. The resulting shifts of the radial NMR peaks are expressed with the ^{15}N peak shifts to the size range of the ^{1}H peak shifts:

$$\Delta\omega_{HN} = \sqrt{\Delta\omega_H^2 + (\Delta\omega_N/5)^2} \quad \text{(Equation 1)}$$

The chemical shift changes of affected proMMP-7 residues were plotted against total dp8 concentrations and dissociation constant K_D fitted by non-linear regression in Origin (Originlab, Northampton, Massachusetts) to a 1:1 model of ligand binding:

$$p_{free} = \frac{\Delta obs}{\Delta max} = \frac{([P]_t + [L]_t + K_D) - \sqrt{([P]_t + [L]_t + K_D)^2 - 4[P]_t[L]_t}}{2[P]_t} \quad \text{(Equation 2)}$$

where $[P]_t$ is the total protein concentration, $[L]_t$ is the total carbohydrate ligand concentration, Δobs is the observed change at this value of $[L]_t$, and Δmax is the maximal change reached upon saturation by the ligand.

3D ^{15}N-separated NOESY-HSQC spectra were collected on both $^{15}N/^{2}H$-labeled proMMP-7 (E195A) alone and with a 1.5-fold molar excess of heparin dp8, using a mixing time of 100 ms. A small number of intermolecular NOEs were identified between the pro-enzyme and anomeric protons of the heparin dp8 resonating between 5 and 6 ppm. These NOEs were absent from the corresponding spectrum of the free state of proMMP-7 (E195A).

Surface Plasmon Resonance

The biotinylated heparin was immobilized to streptavidin chip based on the manufacturer's protocol. For binding analysis, 250 or 1000 nM of pro-MMP7 in 10 mM HEPES (pH 7.5), 10 mM $CaCl_2$, 0.1 mM $ZnCl_2$, and 10 mM 2-mercaptoethanol was flowed over the heparin chip at 30 μL/min at 25°C, followed by 2 min. of flow of the same buffer for dissociation and surface regeneration using 2 M NaCl.

Heparin dp16 Activation of proMMP-7

ProMMP-7 were incubated with increasing concentrations of heparin oligosaccharides dp16 per (Fulcher et al., 2014). The reaction mixtures were incubated for 2 h at 37°C, stopped using SDS-containing gel-loading buffer (Novex), separated on Bis-tris 4–12% SDS-PAGE gels (Novex), and stained with Coomassie Blue. The protein bands were quantified using Quantity One software (Biorad).

Paramagnetic Relaxation Enhancements

From spin-labeled heparin dp8. NMR samples of 300 μM $^{15}N/^{2}H$-labeled proMMP7 (E195A) were studied at 310 K in 20 mM imidazole (pH 6.6), 10 mM $CaCl_2$, 20 μM $ZnCl_2$ and 10 mM 2-mercaptoethanol. Spin-labeled heparin dp8 was titrated to total concentration of 450 μM. Apparent ^{1}H R_2 relaxation rate constants were measured with the spin-labeled dp8 with and without ascorbic acid reduction in order to estimate the PRE as:

$$\Gamma_2 = R_{2,paramag} - R_{2,diamag} \quad \text{(Equation 3)}$$

The relaxation rate constants were measured using a CPMG sequence that suppresses ^{1}H-^{1}H J-couplings (Koppisetti et al., 2014). Two-point fitting of TROSY-detected, amide proton relaxation used relaxation periods of 0 and 10 ms (Iwahara et al., 2007).

Solvent PREs from non-specific Gd ·EDTA probe of surface. Tetrasaccharides were chosen to prevent any binding from bridging to a second enzyme molecule and slowing tumbling. NaCl was omitted from the solutions to enhance affinity for proMMP-7.

Series of CPMG-TROSY NMR spectra were collected as described above to estimate the amide ^{1}H NMR relaxation before and after addition of paramagnetic Gd·EDTA, both in the absence and presence of a 1.5-fold molar excess of heparin dp4 for comparison (Figure 5A), an enhancement of a reported strategy (Arumugam et al., 1998). Apparent ^{1}H R_2 and Γ_2 relaxation rate constants were measured similarly for $^{15}N/^{2}H$-labeled proMMP-7 (E195A) in the absence and presence of 0.3 mM Gd ·EDTA. The difference of the solvent PREs, $\Gamma_{2,\ free}$ - $\Gamma_{2,\ dp4\text{-}bound}$, was taken as the measure of protection of the surface by heparin dp4; see Figure 5.

Restrained Docking of Heparin dp8 to proMMP-7

Explicit distance restraints to the spin-labeled reducing end of heparin dp8 were obtained from the PREs (Γ_2) using an equation of ref (Battiste and Wagner, 2000) simplified by $\omega_H\tau_c >> 1$ to the form (Koppisetti et al., 2014):

$$r = 4K\tau C/\Gamma 2 \quad \text{(Equation 4)}$$

where K is $1.23 \cdot 10^{-44}$ m^6s^{-2}. The rotational correlation time τ_c of protein-heparin complexes was obtained from amide ^{15}N cross-correlation rates η_{xy} (Liu and Prestegard, 2008) interpreted by the spectral density expression used in the TRACT approach (Lee et al., 2006). Upper bounds were set at 15% above the distance estimate. An intermolecular NOE from an arginine backbone amide from

$^{2}H/^{15}N$-labeled enzyme to the anomeric proton H1 of GlcNS6S 5 or 7 had an upper bound of 6 Å. Lower bounds were implicitly at van der Waals distance.

Ambiguous distance restraints from any residue of heparin dp8 to explicit protein amide groups were applied on the basis of amide CSPs from heparin dp8 or protection of amides by heparin dp4 from line broadening by Gd·EDTA with $\Delta\Gamma_2 > 37\ s^{-1}$. Ambiguous distance restraints from any residue of heparin dp8 to basic side chains were also applied on the basis of mutations that impaired activation of proMMP-7 by heparin dp16. The combination of the intermolecular distance restraints from the explicit PRE and NOE measurements and the ambiguous sources were used to dock coordinates of heparin dp8 with the NMR solution structure of human proMMP-7 reported in ref (Prior et al., 2015). CYANA 2.1 (Guntert and Buchner, 2015) was utilized in concert with the intramolecular proMMP-7 NOE-derived distance restraints and chemical shift-derived dihedral restraints of the NMR structure (Prior et al., 2015). CYANA topology files describing the sugar monomers were derived from topology files curated by the Automated Topology Builder (Malde et al., 2011) and based on accession number 9804 for 2-*O*-sulfo-α-*L*-idopyranosyluronic acid (IDS or IdoA2S) and 9778 for *N*,6-*O*-disulfo-glucosamine (SGN or GlcNS6S). The docking simulations required the proMMP-7 polypeptide to be linked to the calcium and zinc ions and heparin dp8 chains via tethers of non-interacting pseudoatoms. With this tethering and flexible structural integrity enforced, the carbohydrate chains were docked with the intermolecular distance restraints. Of 120 structures calculated with heparin dp8 bridging between domains, the 16 with lowest target function were kept, i.e. those agreeing best with the measured distance restraints. Of 160 calculated with heparin dp8 bound to the back of the catalytic domain, the 16 with lowest target function were retained.

To alleviate bad contacts, 150 iterations of Powell energy minimization using Sybyl X 2.1.1 (Certara) were applied to each member of each ensemble. The 24 distance restraints to the zinc and calcium ions (Lang et al., 2001) used for the structure determination (Prior et al., 2015) were present during the minimization to maintain metal coordination. The ensembles were superposed and depicted using Pymol (DeLano, 2002). Average RMSDs to the mean were computed for protein backbone atoms using Molmol (Koradi et al., 1996) and for carbohydrate atoms C1 to C4, O4, and O5 using VMD (Humphrey et al., 1996).

QUANTIFICATION AND STATISTICAL ANALYSIS

The structural coordinates and their variability are represented by 16-member ensembles. The variability is quantified as the average RMSD of the backbone to the mean. The standard deviation of this overall average RMSD variability is listed in Table 1. The mean and standard deviation of triplicate measurements are reported in the binding results of Figure 2 and activation assays of Figure 3.

DATA AND SOFTWARE AVAILABILITY

The solution structural coordinates of proMMP-7 complexes with heparin octasaccharides are deposited under RCSB PDB accession codes 5UE2 and 5UE5.